18,12

The change in the thermal conductivity of a multilayer array of carbon nanotubes during its lateral compression

© A.V. Savin

[1] N.N. Semenov Federal Research Center for Chemical Physics Russian Academy of Sciences, Moscow, Russia
[2] Plekhanov Russian University of Economics, Moscow, Russia

E-mail: asavin@center.chph.ras.ru

Received November 2, 2021
Revised November 14, 2021
Accepted November 18, 2021

Numerical simulation of thermal conductivity across a multilayer array of single-walled carbon nanotubes is carried out. The effect of transverse compression of the array on thermal conductivity has been studied. It is shown that the compression of the array can occur uniformly when all the nanotubes of the array are compressed equally, and it can occur inhomogeneously when a part of the nanotubes is strongly compressed, and the other part is weakly compressed. With homogeneous compression, the thermal conductivity of the array increases, but with inhomogeneous compression, it does not change and may even decrease in case of a large number of layers. This effect is especially pronounced for arrays of nanotubes of small diameter ($D < 2$ nm).

Keywords: carbon nanotubes, nanotube arrays, transverse compression, heat conductivity.

DOI: 10.21883/PSS.2022.03.53194.231

1. Introduction

Carbon nanotubes (CNTs) have the form of a graphene sheet rolled into a cylinder with diameter of 0.4 nm and a length of up to several cm. Topologically similar molecular structures were first obtained by thermal decomposition of carbon monoxide on an iron contact [1]. CNTs themselves as ideal cylindrical macromolecules were obtained much later as by-products of the synthesis of fullerene C_{60} [2]. Interest in CNTs is associated with their unique properties [3,4]. By now, nanotubes with the required geometric properties (i.e., with the desired diameter, length, and chirality) can be easily synthesized [5,6] and used to obtain bundles of parallel CNTs [7,8]. Such materials, also called CNT scaffolds or arrays, have even more superior mechanical properties compared to isolated nanotubes due to van der Waals interactions between them [9].

Isolated CNTs have high thermal conductivity [10–14], their thermal conductivity can reach values above 3000 W/mK. Numerical simulation of heat transfer along an ideal single-walled nanotube shows that the thermal conductivity coefficient increases monotonically with increasing its length [15–17]. Detailed simulation of heat transfer along a nanotube with a chirality index (6,6) showed [18] that the thermal conductivity of an ideal nanotube increases in direct proportion to the logarithm of its length. Macroscopic assemblies of nanotubes, such as their arrays, fibers (bundles) and films, have lower thermal conductivity due to poor nanotube alignment and low density of their packages [19–22]. Films of highly aligned CNTs were obtained in [23], their thermal conductivity can reach values up to 700 W/mK. In a bundle of highly aligned (parallel) nanotubes, the thermal conductivity across the bundle is much lower than the thermal conductivity along the bundle. According to calculations [24], the transverse thermal conductivity of a bundle of parallel CNTs (10,10) has a very low value of 0.05 W/mK, since weak van der Waals bonds are responsible for heat transfer across the bundle and strong valence bonds are responsible for heat transfer along the bundle. The transverse thermal conductivity can be increased by introducing intermolecular valence bridges between adjacent nanotubes [25,26]. Please note that no detailed numerical simulation of heat transfer across multilayer CNT arrays has been carried out (only individual elements of such arrays have been considered).

Nanotubes have high longitudinal (axial) rigidity and relatively weak transverse (radial) one. In view of this, with a sufficiently large diameter, a nanotube due to non-valence interaction of atoms on its surface can pass from a hollow cylindrical shape to a implode (collapsed) state [27–33]. The collapsing of nanotubes should significantly affect the transverse rigidity and thermal conductivity of multilayer arrays of parallel CNTs.

Due to the cavity hollowness of CNTs, their crystals, in contrast to dense materials, can exhibit very high transverse compressibility in the elastic region. This makes it possible to use CNT arrays for shock and vibration protection [34,35]. In this work, we will study the effect of transverse compression of a multilayer array of single-walled nanotubes on its thermal conductivity. It

will be shown that the compression of the array can lead not only to an increase in heat transfer across the array, but also, depending on the degree of compression, to its decrease. To simulate heat transfer, we will use the chain model proposed earlier for modeling of the graphene sheets dynamics [36] and further modified to analyze the structure of an array of CNTs [37]. The simulation of heat transfer across a multilayer array of CNTs at different degrees of its compression will be carried out.

2. Chain model of graphene nanoribbon and nanotube

Let us consider an array of parallel single-walled carbon nanotubes lying between flat multilayer graphene sheets (see Fig. 1). Under transverse compression, the shape of this molecular structure is completely determined by the shape of its cross section. Suppose the nanotubes of the array lie along the z axis, and the graphene sheets bounding the array — be parallel to the xz plane. In the transverse section (in the xy plane), the array of CNTs will have the form of a multilayer system of cyclic chains lying between the linear chains. Therefore, it is convenient to describe the array using the two-dimensional model, in which to graphene sheets correspond the linear molecular chains [36], and nanotubes — the cyclic molecular chains [38].

Under transverse compression, the cross-sectional shape of a nanotube completely describes its deformation. Therefore, the compression of a bundle of parallel nanotubes can be described as a deformation of their cross sections. This approach allows one to significantly reduce the dimensionality of the simulated molecular system. This model has been successfully used earlier to simulate rolls of graphene nanoribbons [36], to winding nanoribbons on nanotubes [38], to transverse compression of a nanotube bundle [37] and to analyze the mechanical properties of single-walled and multi-walled nanotubes located on flat substrates [39,40].

When a graphene sheet (nanoribbon) is section in the zigzag direction, it looks like a homogeneous chain with a step $R_0 = r_c\sqrt{3}/2 = 1.228$ Å ($r_c = 1.418$ Å is the valence bond length C−C). The Hamiltonian of the cross section for the graphene sheet will have the form

$$H_r = \sum_{n=1}^{N_r}\left[\frac{1}{2}M(\dot{\mathbf{u}}_n, \dot{\mathbf{u}}_n) + V(R_n) + U(\theta_n) + W_0(y_n)\right], \quad (1)$$

where the two-dimensional vector $\mathbf{u}_n = (x_n, y_n)$ specifies the coordinates n-th atom of the chain, $M = 12m_p$ — the mass of the carbon atom ($m_p = 1.6603 \cdot 10^{-27}$ kg— proton mass), the number of chain atoms N_r is determined from the nanoribbon length $L = N_r R_0$.

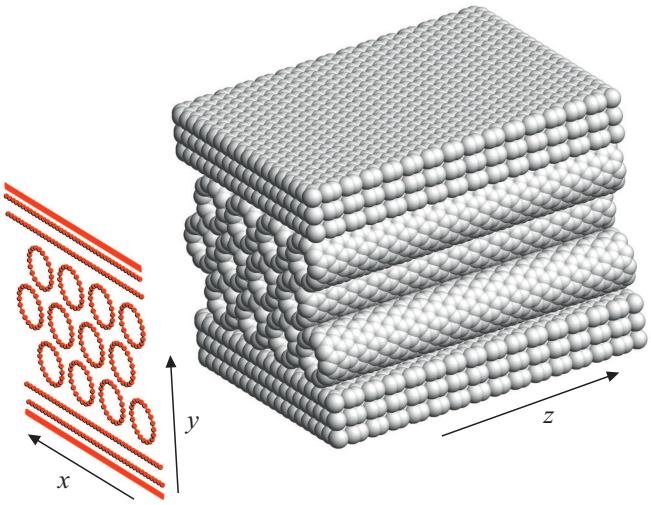

Figure 1. Scheme for 2D model building N_y-layer array of parallel CNTs lying between flat substrates formed by multilayer graphene sheets. There are shown $N_y = 3$ layers of nanotubes with a chirality index (10,0) lying between flat three-layer graphene sheets, and the corresponding 2D model of the system. The CNTs system is compressed along the y axis, and periodic boundary conditions are used along the x axis.

The potential

$$V(R) = \frac{1}{2}K(R - R_0)^2, \quad (2)$$

describes the longitudinal stiffness of the chain, K — the stiffness of the interaction, R_0 — the equilibrium bond length (chain pitch), $R_n = |\mathbf{v}_n|$ — distance between neighboring nodes n and $n+1$ (vector $\mathbf{v}_n = \mathbf{u}_{n+1} - \mathbf{u}_n$).

The potential

$$U(\theta) = \varepsilon_\theta[1 + \cos(\theta)], \quad (3)$$

describes the bending stiffness of the chain, θ — the angle between two adjacent bonds, the cosine of the n-th „valence“ angle $\cos(\theta_n) = -(\mathbf{v}_{n-1}, \mathbf{v}_n)/R_{n-1}R_n$.

The parameters of the potentials (2) and (3) are determined in [36,41] from the analysis of the dispersion curves of the graphene nanoribbon: longitudinal rigidity $K = 405$ N/m, energy $\varepsilon_\theta = 3.5$ eV.

In the Hamiltonian (1), the potential $W_0(y)$ describes the interaction of the chain nodes with the substrate formed by the flat surface of the molecular crystal. We assume that the surface of the substrate coincides with the plane $y = 0$. To determine this potential, the dependence of the interaction energy of the carbon atom with the substrate on its distance y from the flat surface of the crystal was found numerically. Calculations [39,42] showed that the interaction energy $W_0(y)$ can be described with good accuracy by the

Lennard–Jones potential (k, l)

$$W_0(y) = \varepsilon_0[k(d_0/y)^l - l(d_0/y)^k]/(l-k), \qquad (4)$$

where the degree $l > k$, ε_0 is the binding energy of the atom with the substrate, d_0 is the equilibrium distance to the plane of the substrate. For a flat surface of the hexagonal boron nitride's crystal (h-BN), the binding energy $\varepsilon_0 = 0.0903$ eV, the equilibrium distance $d_0 = 3.45$ Å, the powers $l = 10$ and $k = 3.75$.

The cross section of a CNT with the chirality index $(m, 0)$ consists of $N_t = 2m$ carbon atoms, each of which describes the displacements of a straight line of nanotube atoms parallel to the z axis. The Hamiltonian of the cross section of a CNT (for cyclic chain of N_t atoms) will have the form

$$H_t = \sum_{n=1}^{N_t}\left[\frac{1}{2}M(\dot{\mathbf{u}}_n, \dot{\mathbf{u}}_n) + V(R_n) + U(\theta_n) + \frac{1}{2}\sum_{l=1,\ |l-n|>4}^{N_t} W_1(r_{n,l})\right], \qquad (5)$$

where the potential $W_1(r_{n,l})$ describes weak nonvalent interactions of remote nodes of the chain n and l, $r_{n,l} = |u_l - u_n|$ — distance between nodes (the difference of indices $|n-l|$ is determined taking into account the cyclic nature of the chain). This potential will also be used to describe the interaction between nodes of different chains. The non-valence interaction energy of chain nodes can be described with high accuracy [42] by the Lennard–Jones potential (5,11)

$$W_1(r) = \varepsilon_1[5(r_0/r)^{11} - 11(r_0/r)^5]/6, \qquad (6)$$

with equilibrium length $r_0 = 3.607$ Å and interaction energy $\varepsilon_1 = 0.00832$ eV.

3. Model of a limited multilayer array of nanotubes

Let us consider the system of parallel $N_{xy} = N_x N_y$ single-walled CNTs $(m, 0)$ limited above and below by two-layer graphene sheets located between two flat substrates (N_x is the number of nanotubes in one layer parallel to the substrate, N_y is number of layers), see the left side of Fig. 1. Along the x axis, we will use periodic boundary conditions with the period a_x.

Let's the coordinates of the k-th nanoribbon (k-th linear chain, $k = 1, \ldots, 4$) are defined by the $2N_r$--dimensional vector $\mathbf{x}_k = \{(x_{k,n}, y_{k,n})\}_{n=1}^{N_r}$, $N_r R_0 = a_x$. Then the nanoribbon deformation energy

$$P_1(\mathbf{x}_k) = \sum_{n=1}^{N_r}[V(R_{k,n}) + U(\theta_{k,n}) + W(y_{k,n})], \qquad (7)$$

where the interaction energy of the chain nodes with a flat substrate is $W(y_{k,n}) = W_0(y_{k,n})$ for $k = 1.2$ and $W(y_{k,n}) = W_0(h - y_{k,n})$ for $k = 3, 4$. Here, h is the distance between the surfaces of flat substrates, the first two chains interact with the first (lower) substrate, the second two — with the second (upper) substrate.

The coordinates of the k-th cyclic chain, the $(k-4)$-th nanotube, are specified by the $2N_t$-dimensional vector $\mathbf{x}_k = \{(x_{k,n}, y_{k,n})\}_{n=1}^{N_t}$, $N_t = 2m$, $k = 5, 6, \ldots, N_c$, where $N_c = 4 + N_{xy}$ is the number of all chains. Nanotube deformation energy

$$P_2(\mathbf{x}_k) = \sum_{n=1}^{N_t}\left[V(R_{k,n}) + U(\theta_{k,n}) + \frac{1}{2}\sum_{l=1,\ |l-n|>4}^{N_t} W_1(r_{k,n,l})\right]. \qquad (8)$$

Interaction energy of chains (nanoribbons and nanotubes) with coordinates $\mathbf{x}_{k_i} = \{u_{k_i,n}\}_{n=1}^{N_{k_i}}$, $i = 1, 2$,

$$P_3(\mathbf{x}_{k_1}, \mathbf{x}_{k_2}) = \sum_{n_1=1}^{N_{k_1}}\sum_{n_2=1}^{N_{k_2}} W(r_{k_1,n_1;k_2,n_2}), \qquad (9)$$

where the distance between the nodes of the chains is $r_{k_1,n_1;k_2,n_2} = |\mathbf{u}_{k_2,n_2} - \mathbf{u}_{k_1,n_1}|$, the number of links in chains $N_k = N_r$ for $k = 1, \ldots, 4$ and $N_k = N_t$ for $k = 5, \ldots, N_c$.

The potential energy of an array of nanotubes, taking into account the periodic boundary condition along the x axis, will have the form

$$E = \sum_{k=1}^{4} P_1(\mathbf{x}_k) + \sum_{k=5}^{N_c} P_2(\mathbf{x}_k) + P_3(\mathbf{x}_1, \mathbf{x}_2) + P_3(\mathbf{x}_3, \mathbf{x}_4) + \sum_{k_1=1}^{4}\sum_{k_2=5}^{N_c}[P_3(\mathbf{x}_{k_1}, \mathbf{x}_{k_2}) + P_3(\mathbf{x}_{k_1}, \mathbf{x}_{k_2} + a_x\mathbf{e}_x)] + \sum_{k_1=5}^{N_c-1}\sum_{k_2=k_1+1}^{N_c}[P_3(\mathbf{x}_{k_1}, \mathbf{x}_{k_2}) + P_3(\mathbf{x}_{k_1}, \mathbf{x}_{k_2} + a_x\mathbf{e}_x)], \qquad (10)$$

where $2N_t$-dimensional vector $\mathbf{e}_x = \{(1, 0)\}_{n=1}^{N_t}$.

4. Stationary states of a compressed multilayer array of nanotubes

To find the stationary state of a multilayer array of CNTs, it is necessary to solve the problem in the minimum energy of the system

$$E \to \min : \{\mathbf{x}_k\}_{k=1}^{N_c}. \qquad (11)$$

The problem in the minimum energy (11) was solved numerically by the conjugate gradient method. Each stationary state of the array

$$\{[(x^0_{n,k}, y^0_{n,k})]_{n=1}^{N_k}\}_{k=1}^{N_c}$$

will be characterized by specific energy $E_a = E/N_a$, where $N_a = \sum_{k=1}^{N_c} N_k = 4N_r + N_{xy}N_t$ — the total number of

atoms in the chain system, and the pressure on the plane of the substrate

$$P = \frac{1}{2a_x a_z} \sum_{k=1}^{2} \sum_{n=1}^{N_r} [W_0'(h - y_{k+2,n}^0) - W_0'(y_{k,n}^0)],$$

where the prime mark denotes the derivative of the function, $a_z = 3r_c/2$ is the width of the cross section of the CNT array.

The analysis of the possible stationary states of single-walled CNTs on a flat substrate [39] shows that a nanotube with chirality index $(m, 0)$ has only one stable configuration at $m < 32$ and two stable configurations (a configuration with an internal cavity and configuration without a cavity) at $m \geq 32$. Therefore, it should be expected that the packing of nanotubes at $m > 32$ (with a diameter of $D > 2.5$ nm) can have many stable stationary states, which will differ from each other by the fraction of nanotubes in the collapsed state.

Let us consider arrays of nanotubes with three characteristic values of the chirality index $m = 15$, 30, 60 (isolated nanotubes with these indices have diameters $D = 1.17$, 2.35, 4.69 nm).

First, let's consider the array of CNT (15,0) with the number of layers $N_y = 11$, the number of nanotubes in one layer $N_x = 18$ and the period $a_x = 26.765$ nm (number of atoms in the linear chain $N_r = 217$) — see Fig. 2, *a*. The numerical solution of the problem in the energy minimum (11) showed that an 11-layer bounded array of CNTs without compression has the thickness (distance between compressing planes) $h_0 = 16$ nm. By successively decreasing the distance h, when solving the problem in the minimum energy, we will obtain stationary states of an array of CNTs with any value of $h < h_0$.

The characteristic form of the stationary state of the array of CNTs for various values of h is shown in Fig. 2. The dependence of the array energy E_a and the pressure on the substrate walls P on h is shown in Fig. 3, *a, b*. The analysis of the change in the cross section structure of the array with a decrease in its thickness showed that there are two characteristic values $h_1 = 14.9$, $h_2 = 11.3$ nm, at which the type of array of nanotubes compression is changing. For $h > h_1$, uniform compression of all nanotubes occurs, at which they retain their cylindrical shape (see Fig. 2, *a*). For $h_1 < h < h_2$, nanotubes are compressed inhomogeneously, from the start, regions of strongly and weakly compressed nanotubes are formed (see Fig. 2, *b*), and further compression leads to an increase of the first region (see Fig. 2, *c*). For $h < h_2$, the region of weakly compressed nanotubes disappears, and strongly compressed nanotubes are flattening (see Fig. 2, *d, e*). For $h_2 < h < h_1$, the energy of the E_a array increases linearly with decreasing thickness, while the pressure on the walls P remains almost constant.

The dependences of the energy E_a and pressure P on the thickness of the 11-layer array of nanotubes (30.0) also have the similar form (see Fig. 4, *a,b*). Here, the characteristic

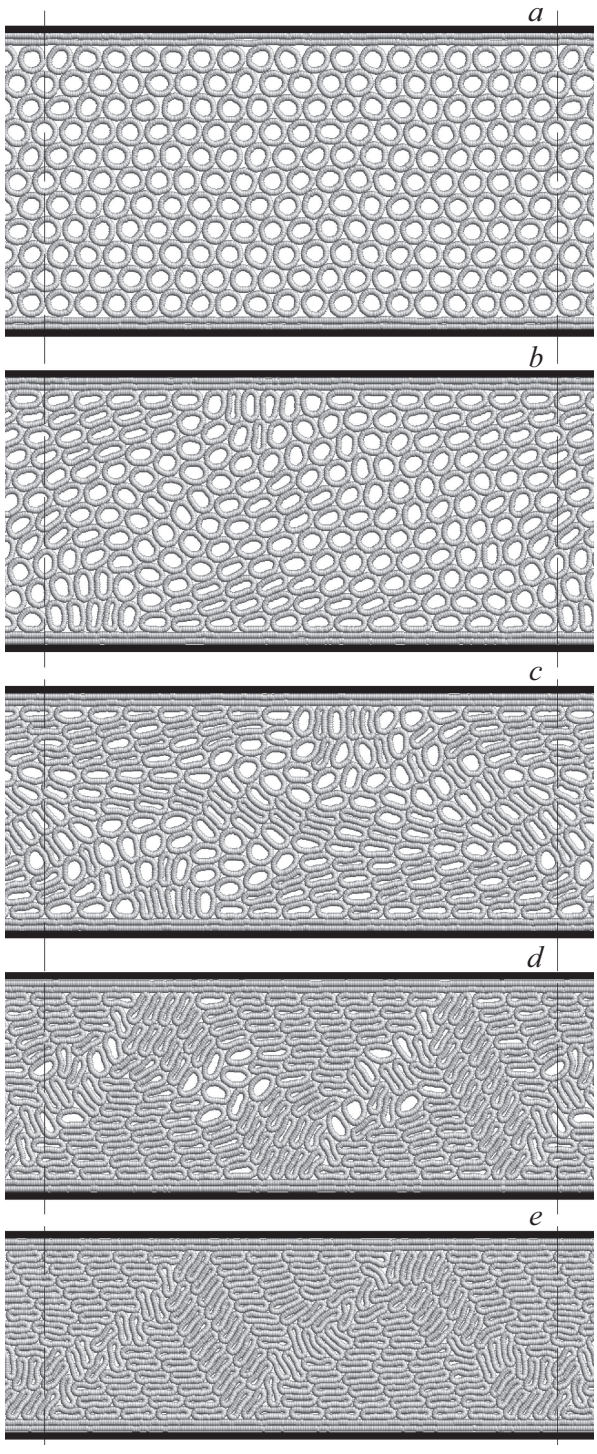

Figure 2. The form of stationary states for the layered structure of $N_x \times N_y$ nanotubes with a chirality index (15.0) and two boundary two-layer graphene sheets (number of nanotubes in one layer $N_x = 18$, number of layers $N_y = 11$, number of links in each cyclic chain $N_t = 30$, the number of links in the linear chain $N_r = 217$) with the distance between the compressive planes of the substrates: (*a*) — $h = 15.87$, (*b*) — 14.27, (*c*) — 12.77, (*d*) — 11.37 and (*e*) — 10.37 nm. Thick horizontal straight lines show contraction planes, dotted vertical ones show boundaries of the periodic cell (period $a_x = 26.765$ nm).

thicknesses are $h_0 = 26.6$, $h_1 = 25.8$ and $h_2 = 15.0$ nm. It should be noted, that the compression of the array of nanotubes (15,0) and (30,0) occurs elastically, when the compressing walls are released, the array always returns to the ground uncompressed state.

The compression of an array of large-diameter nanotubes occurs according to a different scenario, which is associated with their bistability (nanotubes can be in two stable states: in open (cylindrical) and in imploded (collapsed) states). The CNTs array (60.0) is compressed due to the collapsing

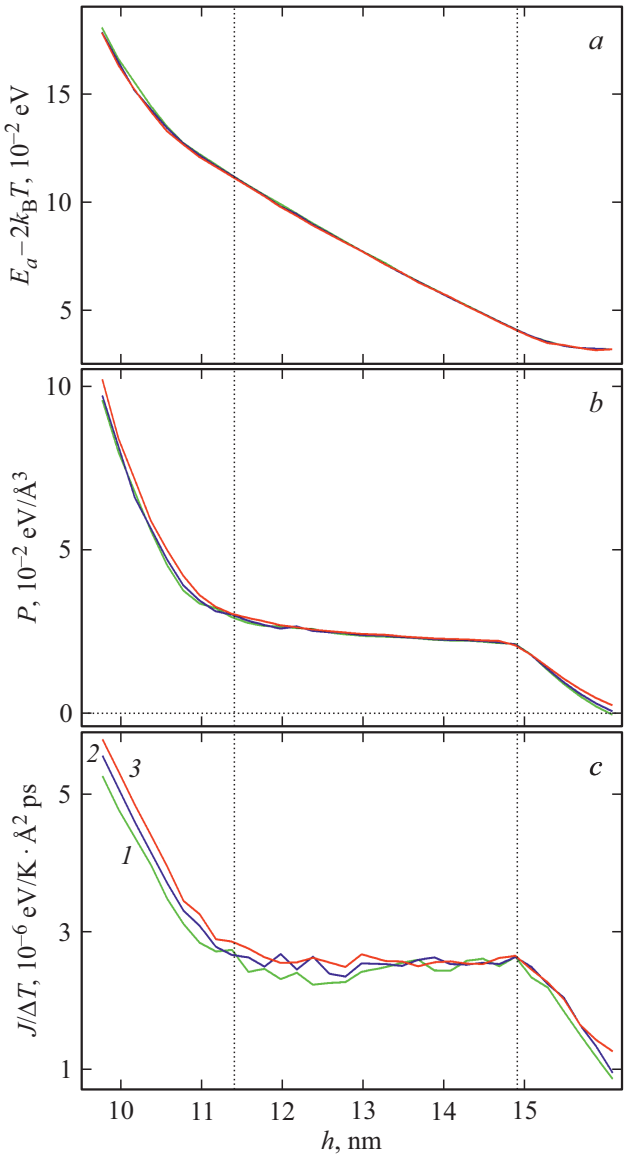

Figure 3. Dependence (a) of specific energy E_a, (b) of pressure P and (c) of heat flux magnitude J for the layered structure $N_x \times N_y$ of nanotubes (15,0) on the distance between the compressing planes h at the temperature of the boundary thermostats $T_\pm = T \pm \Delta T$ ($N_x = 18$, $N_y = 11$, $N_t = 30$, $N_r = 217$, $a_x = 26.765$ nm). Curve *1* defines the dependence for $T_\pm = 150 \pm 15$ K, curve *2* — for $T_\pm = 300 \pm 30$ K, curve *3* — for $T_\pm = 600 \pm 60$ K. The vertical dotted lines show the characteristic values of $h = h_1 = 14.9$ and $h = h_2 = 11.4$ nm.

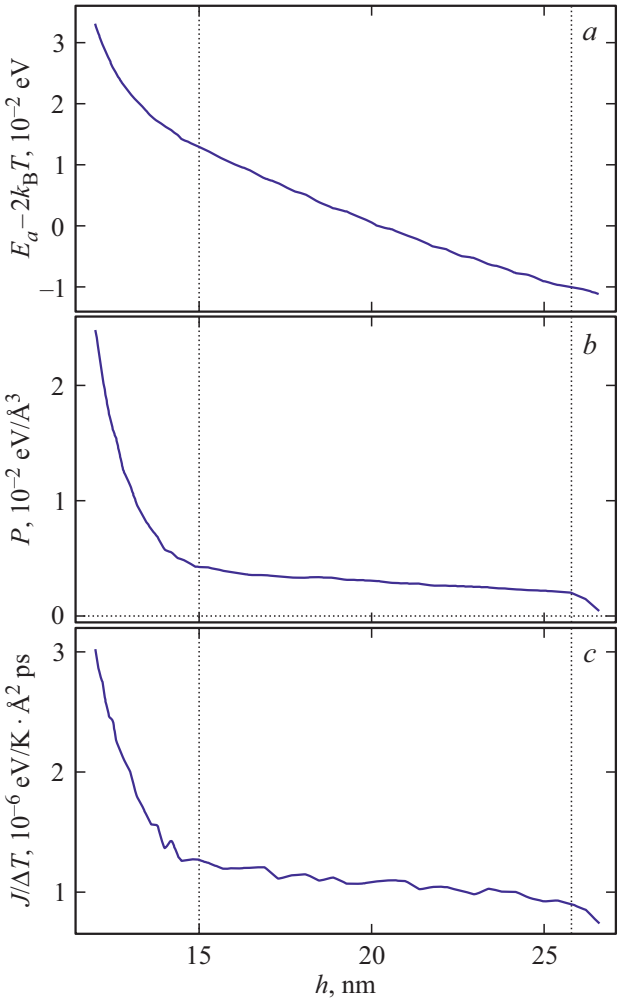

Figure 4. Dependence (a) of specific energy E_a, (b) of pressure P and (c) of heat flux magnitude J for the layered structure $N_x \times N_y$ of nanotubes (30,0) on the distance between the compressing planes h at the temperature of the boundary thermostats $T_\pm = 300 \pm 30$K ($N_x = 18$, $N_y = 11$, $N_t = 60$, $N_r = 392$, $a_x = 48.145$ nm). The vertical dotted lines show the characteristic values of $h = h_1 = 25.8$ and $h = h_2 = 15.0$ nm.

for a part of the nanotubes. The number of collapsed nanotubes increases monotonically with decreasing h, and the energy of the array initially decreases slightly, then also increases, while the pressure on the compressing walls does not change (see Fig. 5, *a, b*). This occurs until the characteristic value of the array thickness $h = h_2$ is reached, at which all nanotubes are already in the collapsed state. Further compression already leads to a sharp increase in energy and pressure.

The array of $N_y = 11$ layers of open nanotubes (60,0) has a thickness of $h_0 = 38.9$ nm. For $h > h_2 = 16$ nm, the array is compressed only due to an increase in the fraction of collapsed nanotubes. Such compression is not elastic, it (only due to the collapse of a part of the nanotubes) transfers the array from one stable state to another one.

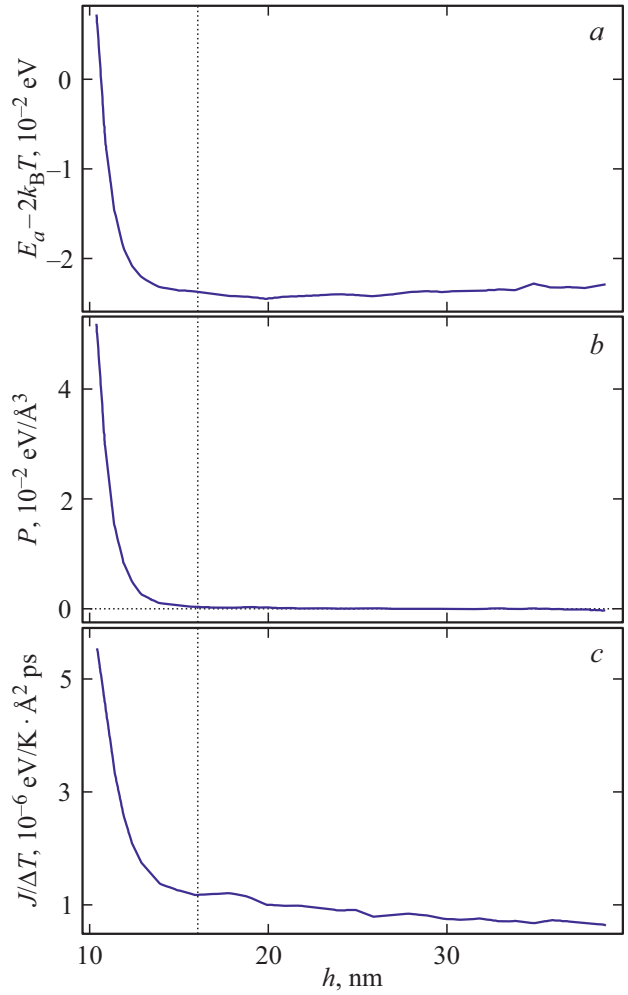

Figure 5. Dependence (a) of specific energy E_a, (b) of pressure P and (c) of heat flux magnitude J for the layered structure $N_x \times N_y$ of nanotubes (60,0) on the distance between the compressing planes h at the temperature of the boundary thermostats $T_\pm = 300 \pm 30$ K ($N_x = 18$, $N_y = 11$, $N_t = 120$, $N_r = 841$, $a_x = 103.294$ nm). The vertical dotted lines show the value of $h = h_2 = 16.0$ nm.

Compression becomes elastic only at $h < h_2$, when all nanotubes in the array are in a collapsed state.

5. Heat transfer transversely the multilayer array of CNTs

Let us simulate heat transfer transversely the multilayer array of CNTs and analyze the dependence of the heat flux on the thickness of the compressed array. To do this, we place the lowest linear chain with number $k = 1$ into the Langevin thermostat with temperature $T_+ = T + \Delta T$, and the topmost chain with $k = 4$ — into the thermostat with temperature $T_- = T - \Delta T$, where T is the average temperature of the system, and $2\Delta T$ is the temperature difference of thermostats.

The dynamics of the considered system of molecular chains is described by the system of Langevin equations

$$M\ddot{\mathbf{x}}_k = -\frac{\partial E}{\partial \mathbf{x}_k} - \Gamma M\dot{\mathbf{x}}_k - \Xi_k, \quad k = 1, 4 \tag{12}$$

$$M\ddot{\mathbf{x}}_k = -\frac{\partial E}{\partial \mathbf{x}_k}, \quad k = 2, 3, 5, 6, \ldots, N_c, \tag{13}$$

where x_k is the $2N_k$-dimensional vector that specifies the coordinates of k-th chain, E is the potential energy of the chain system (10), $\Gamma = 1/t_r$ is the friction coefficient characterizing the intensity of interaction of the outermost linear chains with thermostats (time of particle velocity relaxation due to interaction with the thermostat $t_r = 1$ ps), $\Xi_k = \{(\xi_{k,n,1}, \xi_{k,n,2})\}_{n=1}^{N_r}$ is $2N_r$-dimensional vector of normally distributed random Langevin forces with correlation functions

$$\langle \xi_{k_1,n_1,i}(t_1)\xi_{k_2,n_2,j}(t_2)\rangle = 2Mk_BT_{k_1}\Gamma\delta_{k_1k_2}\delta_{n_1n_2}\delta_{ij}\delta(t_1 - t_2)$$

(k_B is the Boltzmann constant, $T_k = T \pm \Delta T$ is the thermostat temperature).

It is convenient to define the value of the heat flow through the array as the value of the heat flow between the edge linear chains with $k = 1.2$ and $k = 3.4$

$$J_{1,2} = \sum_{n_1=1}^{N_r}\sum_{n_2=1}^{N_r}(\dot{\mathbf{u}}_{2,n_2}, \mathbf{F}_{1,n_1;2,n_2}),$$

$$J_{3,4} = \sum_{n_1=1}^{N_r}\sum_{n_2=1}^{N_r}(\dot{\mathbf{u}}_{4,n_2}, \mathbf{F}_{3,n_1;4,n_2}),$$

where the force vector is

$$\mathbf{F}_{k_1,n_1;k_2,n_2} = (\mathbf{u}_{k_2,n_2} - \mathbf{u}_{k_1,n_1})W_1'(r_{k_1,n_1;k_2,n_2})/r_{k_1,n_1;k_2,n_2},$$

a $r_{k_1,n_1;k_2,n_2} = |\mathbf{u}_{k_2,n_2} - \mathbf{u}_{k_1,n_1}|$ — the distance between node n_1 of chain k_1 and node n_2 of chain k_2.

Let us integrate numerically the system of motion equations (12), (13). As the initial condition, we define the stationary state of the compressed nanotube array $\{\mathbf{x}_k^0\}_{k=1}^{N_c}$ (let us assume that $\{\mathbf{x}_k(0) = \mathbf{x}_k^0,\ \dot{\mathbf{x}}_k(0) = \mathbf{0}\}_{k=1}^{N_c}$). Initially, we integrate the system of motion equations in the course of time t_0 until the linear temperature profile and the stationary heat flux are formed in the array, integrating further, we find the temperature distribution in the chains system

$$T_k = \lim_{t\to\infty}\frac{M}{2N_kk_B(t - t_0)}\int_{t_0}^{t_0+t}\big(\dot{\mathbf{x}}_k(\tau), \dot{\mathbf{x}}_k(\tau)\big)d\tau,$$

$k = 1, 2, \ldots, N_c$, and the value of the specific heat flux through the CNT array

$$J = \langle J_{1,2}\rangle = \langle J_{3,4}\rangle, \tag{14}$$

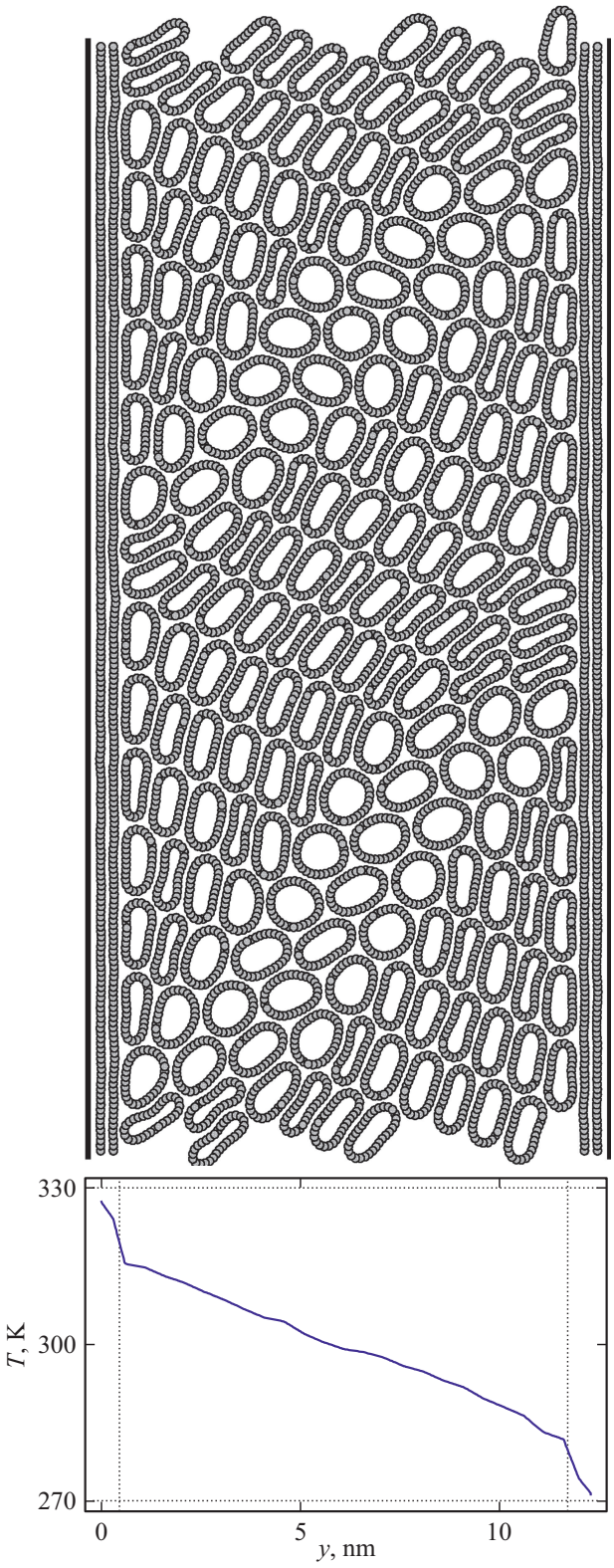

Figure 6. Transverse temperature profile of compressed layered structure of $N_x \times N_y$ nanotubes with the chirality index of (15.0) and two boundary two-layer graphene sheets ($N_x = 18$, $N_y = 11$, $N_t = 30$, $N_r = 217$) at a distance between the compressive planes $h = 12.97$ nm. At the top one period of the layered structure ($a_x = 26.765$ nm) is shown, at the bottom the dependence of the structure temperature T on the transverse coordinate y is shown. Temperature of edge thermostats $T_{\pm} = 300 \pm 30$ K.

where the heat flux between adjacent linear circuits is

$$\langle J_{k_1,k_2} \rangle = \lim_{t\to\infty} \frac{1}{(t-t_0)a_x a_z} \int_{t_0}^{t_0+t} J_{k_1,k_2}(\tau)d\tau.$$

The fulfillment of equality (14) can serve as the criterion for the accuracy of calculations.

The characteristic temperature distribution transversely the multilayer CNT array is shown in Fig. 6. As can be seen in the figure, the linear temperature gradient is formed in the array between the two-layer graphene sheets bounding it.

Numerical simulations of heat transfer showed that the form of the previously obtained dependences of the specific energy E_a and the pressure on the compressing planes P on the distance between them (on the thickness of the CNT array) h is practically independent of the temperature value (see Fig. 3, *a, b*). The heat flux magnitude transversely the array, normalized to the temperature difference of the edge thermostats $J/\Delta T$, also weakly depends on the average temperature value of the array T, but depends significantly on the transverse compression of the array h (see Fig. 3, *c*).

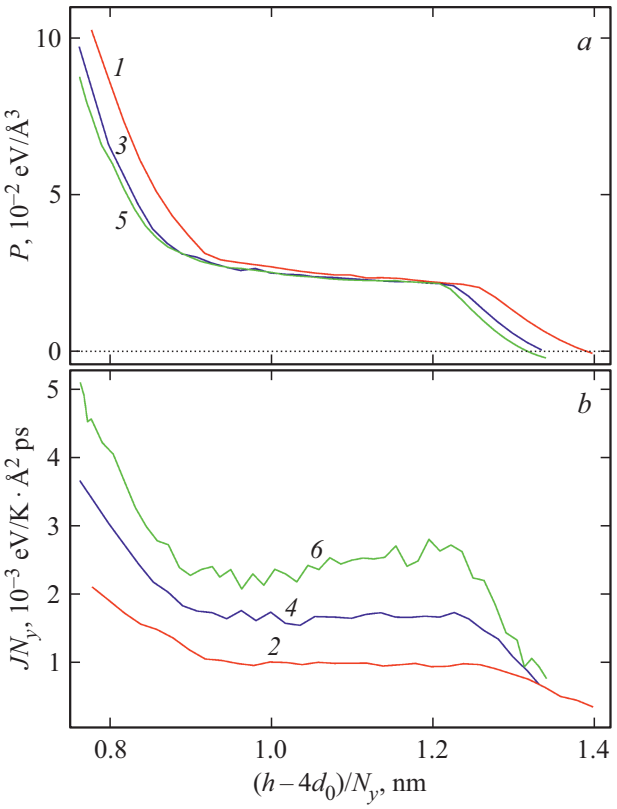

Figure 7. Dependence of (*a*) pressure P and (*b*) multiple of the number of the heat flux layer magnitude JN_y for the layered structure $N_x \times N_y$ of nanotubes (15.0) on relative compression array $(h - 4d_0)/N_y$ at temperature of boundary thermostats $T_{\pm} = 300 \pm 30$K ($N_x = 18$, $N_t = 30$, $N_r = 217$, $a_x = 26.8$ nm). Curves *1* and *2* are for the structure of $N_y = 5$ layers, curves *3* and *4* are for $N_y = 11$, curves *5* and *6* are for $N_y = 22$.

In an array of nanotubes with chirality index of (15.0) (in an array of nanotubes of small diameter) at $h > h_1$ and $h < h_2$, when uniform compression of all nanotubes occurs, the heat flux magnitude J increases linearly with approaching the walls compressing the array (as h decreases). But for $h_2 < h < h_1$, when nonuniform compression of the CNT array occurs, the heat flux magnitude practically does not change when the walls approach each other (see Fig. 3, c). With an increase in the number of layers of nanotubes in the array, the heat flux magnitude can even decrease under transverse compression of the array (see Fig. 7, b). Please note that the dependence of the pressure P on the compressive walls on the relative transverse compression of the array $(h - 4d_0)/N_y$ is practically independent of the number of layers N_y (see Fig. 7, a). It also follows from the figure that, for all values of relative compression, the heat flux magnitude multiplied by the number of layers JN_y increases with the number of layers, i.e., for the considered maximum number of layers $N_y = 22$, the convergence of the transverse thermal conductivity of the CNT array does not occur (with convergence, there should be the finite limit $\lim_{N_y \to \infty} JN_y$).

For (30.0) and (60.0) nanotubes, transverse compression of their multilayer arrays for $h > h_2$ always leads to a slow but linear increase in the heat flux magnitude J (see Fig. 4, c and 5, c). Therefore, it is possible to most effectively change the magnitude of the heat flux during transverse compression only for multilayer arrays of small diameter nanotubes (for CNT (15.0)).

6. Conclusion

The study carried out shows that the transverse compression of a multilayer CNT array can occur uniformly, when all nanotubes in the array are equally compressed, and inhomogeneously, when some of the nanotubes are compressed strongly, and some one are weakly compressed. The uniform compression scenario is realized under weak compression, when all nanotubes remain in the open state, or under very strong compression, when all nanotubes are in the flattened state. With medium compression, the heterogeneous scenario is always realized. Numerical simulation of heat transfer across the array showed that with uniform compression of the array, its thermal conductivity increases. Under inhomogeneous compression of the array, the thermal conductivity does not change, and with the large number of layers of nanotubes, it can even decrease. This effect is most noticeable for nanotube arrays of small diameter ($D < 2\,\text{nm}$).

Funding

This study was financially supported by the Russian Science Foundation (project No. 18-29-19135). Computing resources are provided by the RAS Interdepartmental Center for Supercomputing.

Conflict of interest

The author declares that he has no conflict of interest.

References

[1] L.V. Radushkevich, V.M. Lukyanovich. Russian Journal of Physical Chemistry **26**, *1*, 88-95 (1952).
[2] S. Iijima. Nature **354**, 56 (1991).
[3] A.V. Eletsky. Physics-Uspekhi **172**, *4*, 401 (2002).
[4] D. Qian, G.J. Wagner, W.K. Liu, M.-F. Yu, R.S. Ruoff. Appl. Mech. Rev. **55**, 495 (2002).
[5] J. Di, S. Fang, F.A. Moura, D.S. Galvao, J. Bykova, A. Aliev, M.J.d. Andrade, X. Lepro, N. Li, C. Haines, R. Ovalle-Robles, D. Qian, R.H. Baughman. Adv. Mater. **28**, 6598 (2016).
[6] Y. Bai, R. Zhang, X. Ye, Z. Zhu, H. Xie, B. Shen, D. Cai, B. Liu, C. Zhang, Z. Jia, S. Zhang, X. Li, F. Wei. Nature Nanotechnology **13**, 589 (2018).
[7] B.C. Liu, T.J. Lee, S.H. Lee, C.Y. Park, C.J. Lee. Chem. Phys. Lett. **377**, 55 (2003).
[8] Y. Li, X. Zhang, X. Tao, J. Xu, W. Huang, J. Luo, Z. Luo, T. Li, F. Liu, Y. Bao, H.J. Geise. Carbon **43**, *2*, 295 (2005).
[9] E.G. Rakov. Uspekhi khimii **82**, *1*, 27 (2013) (in Russian).
[10] C. Yu, L. Shi, Z. Yao, D. Li, A. Majumdar. Nano Lett. **5**, *9*, 1842 (2005).
[11] E. Pop, D. Mann, Q. Wang, K. Goodson, H. Dai. Nano Lett. **6**, *1*, 96 (2006).
[12] Q. Li, C. Liu, X. Wang, S. Fan. Nanotechnology **20**, *14*, 145702 (2009).
[13] M.T. Pettes, L. Shi. Adv. Funct. Mater. **19**, *24*, 3918 (2009).
[14] B. Kumanek, D. Janas. J. Mater. Sci. **54**, *10* 7397 (2019).
[15] G. Zhang, B. Li. J. Chem. Phys. **123**, 114714 (2005).
[16] J.R. Lukes, H. Zhong. J. Heat Transfer. **129**, *6*, 705 (2007).
[17] A.V. Savin, B. Hu, Y.S. Kivshar. Phys. Rev. B, **80**, 195423 (2009).
[18] A.V. Savin, O.I. Savina. Physics of the Solid State **61**, *2*, 409 (2019).
[19] S. Badaire, V. Pichot, C. Zakri, P. Poulin, P. Launois, J. Vavro, C. Guthy, M. Chen, J.E. Fischer. J. Appl. Phys. **96**, *12*, 7509 (2004).
[20] A.E. Aliev, C. Guthy, M. Zhang, S. Fang, A.A. Zakhidov, J.E. Fischer, R.H. Baughman. Carbon **45**, *15*, 2880 (2007).
[21] A. Duzynska, A. Taube, K.P. Korona, J. Judek, M. Zdrojek. Appl. Phys. Lett. **106**, *18*, 183108 (2015).
[22] F. Lian, J.P. Llinas, Z. Li, D. Estrada, E. Pop. Appl. Phys. Lett. **108**, *10*, 103101 (2016).
[23] H. Zhan, Y.W. Chen, Q.Q. Shi, Y. Zhang, R.W. Mo, J.N. Wang. Carbon **186**, 205 (2022).
[24] W.J. Evans, M. Shen, P. Keblinski. Appl. Phys. Lett. **100**, 261908 (2012).
[25] M.R. Gharib-Zahedi, M. Tafazzoli, M.C. Bohm, M. Alaghemandi. J. Chem. Phys. **139**, 184704 (2013).
[26] J. Wang, D. Chen, J. Wallace, J. Gigax, X. Wang, L. Shao. Appl. Phys. Lett. **104**, 191902 (2014).
[27] N.S. Chopra, L.X. Benedict, V.H. Crespi, M.L. Cohen, S.G. Louie, A. Zettl. Nature **377**, *14*, 135 (1995).
[28] G. Gao, T. Çağin, W.A. Goddard III. Nanotechnology **9**, 184 (1998).
[29] J. Xiao, B. Liu, Y. Huang, J. Zuo, K.-C. Hwang, M.-F. Yu. Nanotechnology **18**, 395703 (2007).
[30] T. Chang. Phys. Rev. Lett. **101**, 175501 (2008).

[31] J.A. Baimova, Q. Fan,1 L. Zeng, Z. Wang, S.V. Dmitriev, X. Feng, K. Zhou. J. Nanomater. **2015**, 186231 (2015).
[32] A. Impellizzeri, P. Briddon, C.P. Ewels, Phys. Rev. B **100**, 115410 (2019).
[33] M.M. Maslov, K.S. Grishakov, M.A. Gimaldinova, K.P. Katin. Fuller. Nanotub. Car. Nanostructures **28**, 97 (2020).
[34] A.Y. Cao, P.L. Dickrell, W.G. Sawyer, M.N. Ghasemi-Nejhad, P.M. Ajayan, Science **310**, 1307 (2005).
[35] L.K. Rysaeva, E.A. Korznikova, R.T. Murzaev, D.U. Abdullina, A.A. Kudreyko, J.A. Baimova, D.S. Lisovenko, S.V. Dmitriev. Facta Univ. Ser. Mech. Eng. **18**, 1 (2020).
[36] A.V. Savin, E.A. Korznikova, S.V. Dmitriev. Phys. Rev. B **92**, 035412, (2015).
[37] E.A. Korznikova, L.K. Rysaeva, A.V. Savin, E.G. Soboleva, E.G. Ekomasov, M.A. Ilgamov, S.V. Dmitriev. Materials **12**, 3951 (2019).
[38] A. Savin, E. Korznikova, S. Dmitriev, E. Soboleva, Comp. Mater. Sci. **135**, 99 (2017).
[39] A.V. Savin, O.I. Savina. Physics of the Solid State **61**, *11*, 2257 (2019).
[40] A.V. Savin, O.I. Savina. Physics of the Solid State **63**, *1*, 137 (2021).
[41] A.V. Savin, E.A. Korznikova, S.V. Dmitriev. Physics of the Solid State **57**, *11*, 2278 (2015).
[42] A.V. Savin, E.A. Korznikova, S.V. Dmitriev. Phys. Rev. B **99**, 235411 (2019).